Structural characteristics and corrosion behavior of biodegradable Mg–Zn, Mg–Zn–Gd alloys

J. Kubásek · D. Vojtěch

Abstract In this research, binary Mg–Zn (up to 3 wt% Zn) and ternary Mg–Zn–Gd (up to 3 wt% Gd, 3 wt% Zn) alloys were prepared by induction melting in an argon atmosphere. The structures of these alloys were characterized using light and scanning electron microscopy, energy dispersive spectrometry, X-ray diffraction and X-ray fluorescence. In addition, Brinell hardness measurements were taken to supplement these studies. Corrosion behavior was evaluated by immersion tests and potentiodynamic measurements in a physiological solution (9 g/l NaCl). Depending on the composition, structures of the as-cast alloys contained α-Mg dendrites, MgZn, Mg_5Gd and $Mg_3Gd_2Zn_3$ phases. Compared to pure Mg, zinc improved the corrosion resistance of binary Mg–Zn. Gadolinium also improved the corrosion resistance in the case of Mg–1Zn–3Gd alloy. The highest corrosion rate was observed for Mg–3Zn–3Gd alloy. Our results improve the understanding of the relationships between the structure and corrosion behavior of our studied alloy systems.

1 Introduction

Biodegradable materials can gradually dissolve in the human body without the production of toxic compounds [1]. These materials are suitable candidates for medical implants, such as fixation devices for fractured bones or stents [2]. Compared to permanent implants produced from stainless steels, titanium and cobalt-based alloys, a second surgery is not needed to remove the biodegradable implant. Polymeric and ceramic biodegradable materials are not suitable for implantation because of their low mechanical strength and fracture toughness [3]. Metallic materials with higher strength and fracture toughness are suitable candidates for load-bearing applications, such as screws and plates for bone fixation [4]. Magnesium and its alloys have attracted the greatest interest among the biodegradable metallic materials because magnesium itself is a non-toxic element that plays an important role in many biological processes such as those affecting the functions of the muscles, the nerves and the heart as well as the growth of bones. The recommended dietary allowance (RDA) of magnesium for adults is 300–400 mg, which is a significantly higher amount than the other elements [5]. In addition, the strength and Young's modulus of magnesium alloys are close to those of human bone, which supports good healing processes [1, 2, 6, 7]. The main disadvantage of magnesium and its alloys is their high corrosion rates, which influence the amount of hydrogen gas and metal ions released into solution and increase in pH that affect some pH balances in organism [1, 8–12]. Corrosion resistance of magnesium in a physiological environment that contains chloride anions is quite poor, even in the case of pure magnesium. The incorporation of impurities can significantly increase the corrosion rate. Thus, it is necessary to find a magnesium alloy with an acceptable corrosion rate and non-toxic alloying elements. For this purpose, magnesium alloys such as the AZ, AM, AE, ZE, WE, MZ, WZ, LAE [1, 3, 8] series of engineering materials used in the automotive and aerospace industry were studied. Currently, only the WE43 alloy has been used for vascular stents in the human body [13–15].

Mg-RE based alloys are promising candidates for biodegradable implants because RE elements can strengthen magnesium alloys, improve creep resistance at elevated

J. Kubásek (✉) · D. Vojtěch
Department of Metals and Corrosion Engineering, Institute of Chemical Technology, Prague, Technická 5, 166 28 Prague 6, Czech Republic
e-mail: kubasekj@vscht.cz

temperatures [16, 17] and generally slow down corrosion rate [18, 19]. The main influence on the corrosion rate is attributed to interactions of RE with cathodic impurities such as Fe, Ni, Co. These impurities may lead to the formation of intermetallic phases that are more noble than pure magnesium. As a result, galvanic corrosion may be reduced [14]. In some cases, RE elements may increase this protective effect because of their incorporation into the magnesium hydroxide surface layer [12]. Although some RE, such as Pr, Ce and Lu [1], are toxic, others like Gd and Y are acceptable alloying elements at low concentrations [20].

Zinc is an essential element that supports immune functions, protein and DNA synthesis, normal growth and a proper sense of taste and smell [21, 22]. When the magnesium is alloyed, zinc has been shown to improve the corrosion resistance and strength of the material. With a RDA of 10–15 mg/day [23] for adults, the consumption of zinc in higher than these values is generally considered relatively non-toxic. Recently, different zinc containing alloys such as Mg–Zn, Mg–Zn–Y, Mg–Zn–Mn–Ca have been investigated [21, 24–28]. Specifically, amorphous Mg–Zn–based alloys that contained approximately 50 wt% zinc exhibited high corrosion resistance and good biocompatibility in animals [29, 30]. However, the preparation of bulk amorphous Mg alloys is difficult because they need to be cooled at high rates.

Ternary alloys of Mg–Y–Zn that consist of I- or W-phases demonstrate superior mechanical properties and high corrosion resistance [18, 31]. Various Mg–Gd–Zn based alloys were also investigated because [31–36] the high solubility of Gd in Mg (23.49 wt% at 821 K) in contrast with 3.82 wt% at 473 K offers an ideal system for precipitation hardening [35]. Addition of Zn to Mg–Gd based alloys improves their mechanical and creep properties [32], which is correlated to the precipitation of quasicrystals and Laves phases in the structure [33, 34]. Different intermetallic phases may also be present in the Mg–Gd–Zn system depending on the actual composition. The volume fraction of the I-phase has been shown to affect the tensile strength and elongation because of its high symmetry and low interface energy [36]. The formation of the I-phase, however, is influenced by the ratio of Zn/Gd and cooling rate [31, 37, 38]. These mechanical properties

make the Mg–Gd–Zn alloys suitable for biodegradable implants. Although there is still a lack of information about the corrosion behavior of these alloys, especially in simulated body fluids, finding an optimal combination of Mg, Zn and Gd could lead to the preparation of an alloy with corrosion rates acceptable for bone implants.

In this study we focused our attention on the relationship between the structure and corrosion behavior of as-cast Mg–Zn and Mg–Gd–Zn alloys in physiological solution. The influence of Gd on the corrosion resistance of the Mg–Zn system, where the concentration of Zn is limited to 3 wt%, [28, 39–41] is discussed. All of the determined properties were compared with those of pure magnesium.

2 Materials and methods

In this study Mg, two binary Mg–Zn and two ternary Mg–Gd–Zn alloys were investigated. The designations and chemical compositions of the studied alloys are given in Table 1. Cylindrical ingots of Mg, Mg–1Zn, Mg–3Zn, Mg–1Zn–3Gd and Mg–3Zn–3Gd were prepared by melting pure Mg (99,9 wt%), Gd (99.9 wt%), Y (99.9 wt%) and Zn (99.9 wt%) in an induction furnace under an argon atmosphere of technical purity (99.9 wt%). The melt was homogenized for 15 min at 750 °C and cast into cast-iron metal molds that were 100 mm in length and 20 mm in diameter. These molds were not preheated. Chemical compositions of the ingots were verified by taking X-ray fluorescence spectrometry at the center of the ingots (Table 1.). Moreover, part of the prepared ingot was dissolved in diluted solution of nitric acid (8 wt%) and this solution was than analysed using ICP-MS (Inductively Coupled Plasma-Mass Spectrometry). The solution of Nitric acid was prepared from deionized water and Nitric acid for ultra low trace metal analysis. This method allow the accurate determination of the concentration of impurities, such as (Fe, Ni, Cu) that negatively affect the corrosion resistance of magnesium alloys. Brinell hardness measurements were performed on samples ground with P800 abrasive paper using a load of 15,625 kg (HBW 2.5/15.625). The microstructure of the alloys was observed by optical microscopy and scanning electron microscopy

Table 1 Chemical compositions of the investigated alloys (in wt%)

Alloy	Mg	Zn	Gd	Mn	Fe	Cu	Ni	Al
Mg	99.95	0.01	–	<0.01	<0.004	<0.004	<0.004	0.04
Mg–1Zn	99.05	0.90	–	0.03	<0.004	<0.004	<0.004	0.02
Mg–3Zn	97.49	2.46	–	0.04	<0.004	0.01	<0.004	<0.01
Mg–1Zn–3Gd	96.19	0.78	2.78	0.02	<0.004	<0.004	<0.004	0.3
Mg–3Zn–3Gd	94.94	2.62	2.39	0.02	<0.004	<0.004	<0.004	<0.01

(Tescan Vega 3 LMU, equipped for energy dispersive spectrometry EDS, (Oxford Instruments Inca 350). For this purpose, the samples were grinded using SiC abrasive papers (P180–P4000), polished by diamond pastes with 2 and 0.7 μm particles and etched in a 2 ml HNO_3 + 100 ml H_2O solution. Phase and chemical compositions were studied by energy dispersion spectrometry (Oxford Instruments Inca 350) and X-ray diffraction (X'Pert Philips, 30 mA, 40 kV, X-ray radiation Cu K_α).

Corrosion behavior was studied by immersion tests that were performed in a simulated physiological environment (9 g/l NaCl solution) at an initial pH of 6.5. Samples were first ground with SiC abrasive papers (P4000) and degreased with ethanol. Then, coupons of the samples that were approximately 20 mm in diameter and 2 mm thick were immersed in the solution for 168 h at 20 °C. To prevent evaporation of the corrosion media, the corrosion chamber was closed during the tests. The ratio of the volume of physiological solution to the surface area of each specimen was kept at 36 ml/cm^2. Corrosion products were removed using a solution of 200 g/l CrO_3, 10 g/l $AgNO_3$ and 20 g/l $Ba(NO_3)_2$, according to ISO 8407. Corrosion rates were calculated from the weight losses measured at an accuracy of 0.1 mg. Each immersion test was performed three times to ensure sufficient statistics. Polarization curves were measured in a simulated physiological environment (9 g/l NaCl solution) at an initial pH of 6.5 on a FAS1 Gamry using a SCE (Ag/AgCl/KCl: 3 mol/l) as the reference electrode and a platinum wire as the counter electrode. These tests were carried out on cylindrical samples with 10 mm in diameter and 10 mm high. Specimens with screw-thread were kept immersed in the solution by Teflon holder. The ratio of the volume of physiological solution to the surface area of each specimen was kept at the same level as in the case of immersion tests. Cathodic polarization curves were scanned from 0.2 V(Eocp) to the negative values of potential versus Eocp at a rate of 1 mV/s after 1 h and 24 h immersion.

3 Results

3.1 Structure and hardness

Detailed views of the structures of the as-cast binary Mg–Zn and ternary Mg–Zn–Gd alloys were taken by SEM (Fig. 1). All the alloys contained dendritic patterns where the average thickness of the dendrite arms were 15–20 μm and were similar for all the materials. Both binary Mg–Zn and Mg–1Zn–3Gd alloy were characterized by obvious dendritic microsegregations. The dendrite cores have a dark contrast in the figures because they were depleted by Zn and Gd. The dendrite edges, which were enriched with Zn and Gd, appear light. In this work at least 50 point analyses using EDS were applied to the individual phases in the alloys. The average

concentration and standard deviations of Zn and Gd elements in different phases of studied magnesium alloys are showed on Fig. 2. Differences in Zn concentrations between the cores and edges of the dendrites increased from 1.5 ± 0.3 to 5 ± 0.9 wt% for the Mg–1Zn and Mg–3Zn alloys, respectively (Fig. 2); however, nearly no difference in concentration of Zn in the cores and edges of the dendrites was observed for the Mg–1Zn–3Gd alloy. In this case, the dendritic microsegregations were caused only by the 1.5 wt% concentration difference of Gd. Finally, no measurable Gd or Zn gradient in the solid solution of α-Mg was observed in Mg–3Zn–3Gd alloy. All alloys were prepared by casting to the non-preheated brass mould. Due to the rapid cooling rate, the structures of alloys were in nonequilibrium state and contain some intermetallic phases. The light particles randomly distributed at the edges of the dendrites in the Mg–Zn binary alloys (Fig. 1) were determined as MgZn eutectic phases [21]. These phases were observed in Mg–1Zn, although maximum solid solubility of zinc in magnesium at laboratory temperature is slightly higher than 1 wt% [21]. The concentration of Zn in MgZn phases rose from 18.5 ± 6.5 to 34 ± 5.6 for Mg–1Zn and Mg–3Zn respectively. The averaged diameter of spherical particles was only about 1 μm for Mg–1Zn and from 2 to 4 μm for Mg–3Zn (Fig. 1). During the EDS measurements, the vicinity of the analysed point to a distance from 1 to 2 μm influences the results. Therefore, chemical composition of MgZn phases in Mg–1Zn alloy is influenced partially by surrounding solid solution and resulting concentration of Zn is lowered for Mg–1Zn alloy. According to the phase diagram for Mg–Zn binary system the maximum solid solubility, eutectic point and concentration of Zn in MgZn phase is about 6.2 wt%, 51.3 and 74.4 wt% respectively. So the concentration measured for observed phases lies in the two phase (α-Mg and MgZn) region nearly at the eutectic composition [21]. X-ray diffraction analyses were used to confirm the existence of this phase in the structure of Mg–Zn binary alloys; however, MgZn phase was detected only in the case Mg–3Zn alloy (Fig. 3). We assume that the amount of MgZn phase in Mg–1Zn is behind the detection limit of XRD. In the Mg–1Zn–3Gd alloy low amount of small light particles with approximately 22.5 ± 5.1 wt% of Gd and 1.5 ± 1.2 wt% of Zn were characterized as a eutectic mixture of Mg_5Gd and α-Mg. The amount of these phases in magnesium was also behind the detection limit for XRD analyses that showed only the presence of α-Mg.

The Mg–3Zn–3Gd alloy consisted of a nearly continuous network of secondary phases along the dendrite edges (Fig. 1d, h). These phases (Fig. 2b) contained 13 ± 2.5 wt% of Zn and 15.7 ± 2.6 wt% of Gd, which correlates to the $Mg_3Gd_2Zn_3$ phase [40, 42]. Moreover, this ternary alloy contained some small, irregularly distributed particles with higher concentration of Gd ($30.6 \pm$

Fig. 1 Microstructure of investigated alloys (SEM views) **a**, **e** Mg–1Zn, **b**, **f** Mg–3Zn, **c**, **g** Mg–1Zn–3Gd, **d**, **h** Mg–3Zn–3Gd
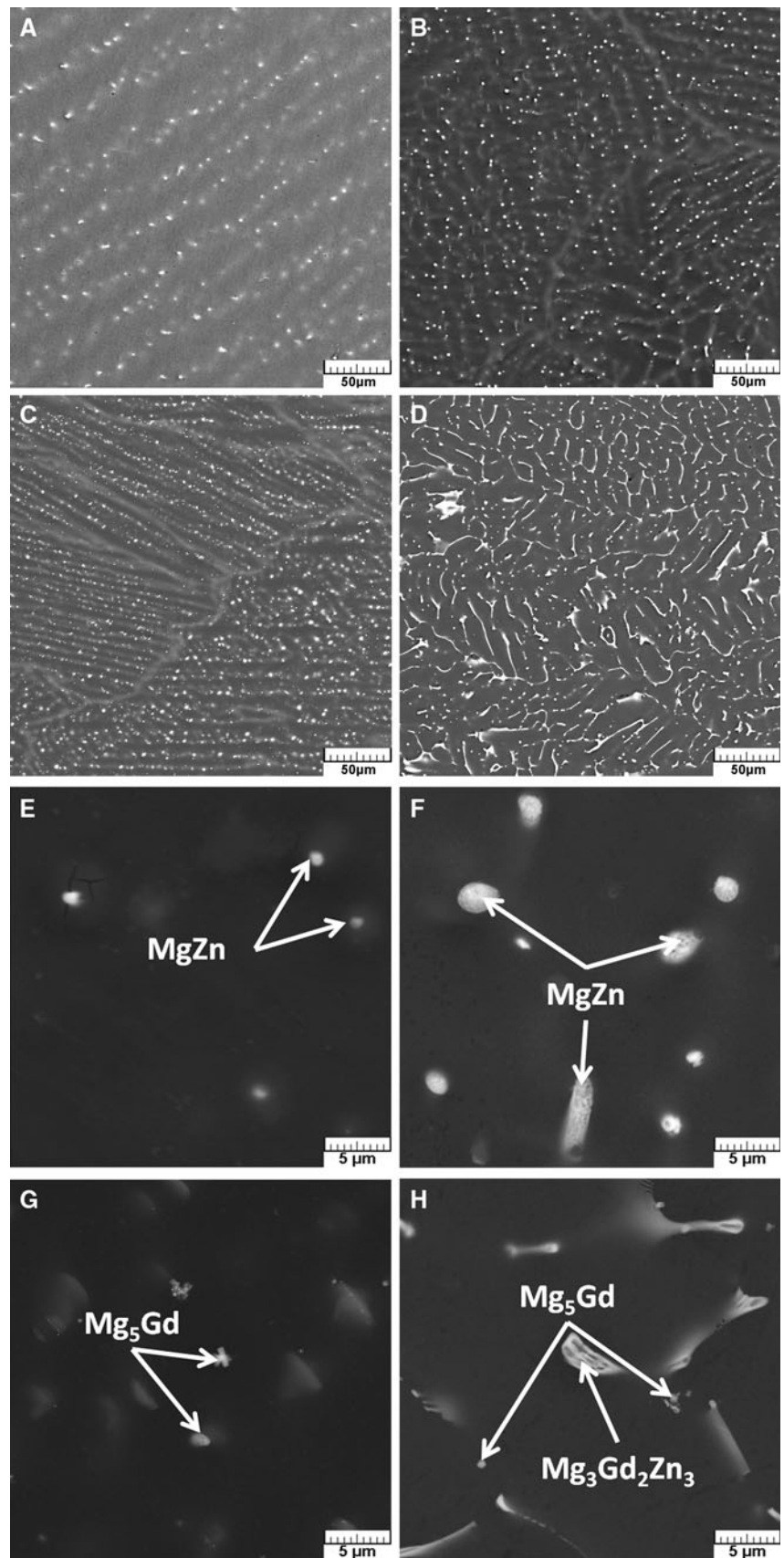
Fig. 2 Composition of solid solution and phases of investigated alloys **a** Zn concentration, **b** Gd concentration (Color figure online)
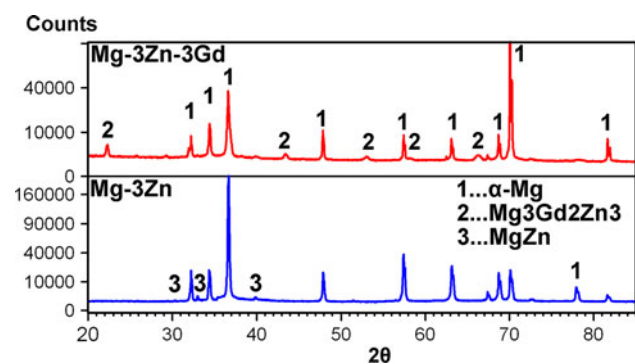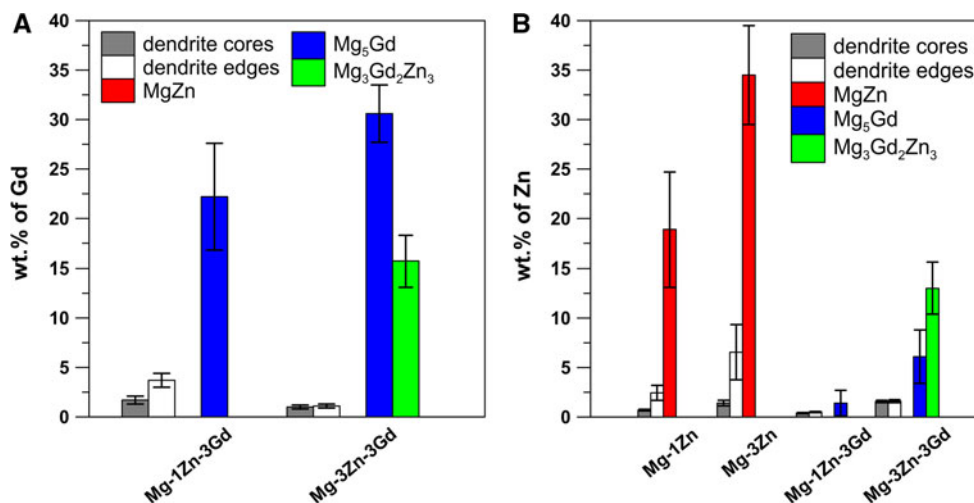

Fig. 3 X-ray diffraction analyses of Mg–3Zn–3Gd and Mg–3Zn alloy

Fig. 4 Brinell hardness (HBW 2.5/15.625) of investigated alloys

2.9 wt%) and a low concentration of Zn (6.1 ± 2.7 wt%). These particles correspond to the Mg_5Gd eutectic phases [17, 19]. XRD analyses confirmed the presence of $Mg_3Gd_2Zn_3$ phase (W-phase) (Fig. 3); however, Mg_5Gd phase was not detected by XRD due to its low amount in the structure of the Mg–3Zn–3Gd alloy. For all investigated alloys, the volume fraction of secondary phases was increased with increasing concentrations of Zn and Gd in alloy. Furthermore, the Brinell hardness of Mg–Zn and Mg–Zn–Gd alloys was increased with Zn and Gd concentration from approximately 26 HBW for pure Mg up to 45 HBW for the Mg–3Zn–3Gd alloy (Fig. 4).

3.2 Corrosion behavior

3.2.1 Immersion tests

Corrosion rates of the studied materials are shown in Fig. 5. Compared to pure magnesium, the corrosion rates of binary Mg–Zn alloys are significantly lower, where the minimum corrosion rate is observed for the Mg–1Zn alloy (1.3 mm/y). Increasing the Zn content to 3 wt% leads to a
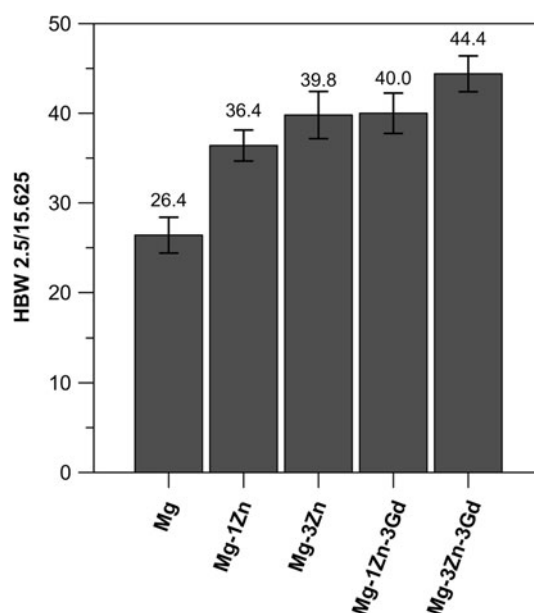
reduction in corrosion resistance. The reason for this behavior will be discussed later. The addition of 3 wt% of gadolinium to the Mg–1Zn binary alloy, however, increases corrosion resistance, decreasing the corrosion rate to approximately 0.8 mm/y. The Mg–1Zn–3Gd alloy shows the best corrosion resistance among all the investigated materials. In contrast, the Mg–3Zn–3Gd ternary alloy is characterized with the worst corrosion resistance of all the studied materials, exhibiting a corrosion rate that is nearly twice that of pure magnesium (5.3 mm/y).

3.2.2 Corrosion products after immersion tests

Figure 6 shows the surfaces of the corroded alloys after immersion in NaCl solution. After immersion tests, the
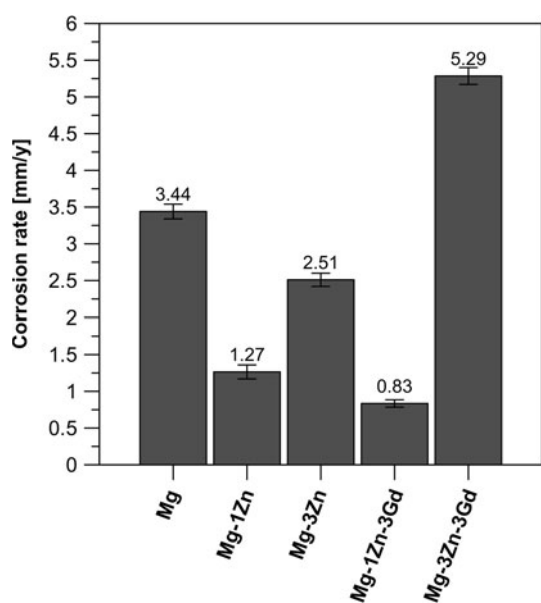
Fig. 5 Corrosion rates of the investigated alloys

surfaces of all the samples are covered by corrosion products, which are composed of globular particles. These particles form a compact layer on only the Mg–1Zn–Gd alloy whereas deep pits are clearly visible in the other alloys. XRD analysis confirmed the presence of $Mg(OH)_2$ on the surface of all studied alloys, and EDS analyses provided complementary results further verifying the chemical composition of the corrosion products. Mg, O and approximately 0.2 wt% of Zn is present on the surface of the Mg–Zn binary alloys and only Mg and O is seen on the Mg–Gd–Zn alloys; however, 0.2 wt% of zinc is near the lower detection limit of EDS and should be interpreted carefully. Overall, these results confirm that the corrosion product is magnesium hydroxide. Figure 7 depicts the surface of the corroded alloys after removing the corrosion products by soaking in 200 g/l CrO_3, 10 g/l $AgNO_3$ and 20 g/l $Ba(NO_3)_2$ solution. Pits cover the surfaces of the Mg–3Zn and Mg–3Zn–3Gd alloys, and the number of pits, their size and distribution across the surface depends on the chemical composition of the alloy. The Mg–1Zn–3Gd alloy has the lowest corrosion rate and contains no large pits on the surface, (Fig. 7). In contrast, the surface of Mg–3Gd–3Zn, the alloy with the highest corrosion rate, consists of a large number of deep pits that are distributed irregularly over the surface. Overall, the measured corrosion rate of the Mg–3Zn–3Gd alloy is double that of the binary Mg–3Zn alloy, which is consistent with the quality of the surface observed for the Mg–3Zn–3Gd alloy. Magnesium surface layer looks like quite regular compared to some studied magnesium alloys after corrosion exposures. However, it is evident from Fig. 7e that the surface after removing of corrosion products is quite irregular with

many signs of local corrosion. This fact is in good agreement with established higher corrosion rate of magnesium compared to binary Mg–1Zn, Mg–3Zn and Mg–1Zn–3Gd alloy.

3.2.3 Potentiodynamic measurements

The potentiodynamic polarization curves of the alloys after 1 and 24 h immersion in physiological solution are shown in Fig. 8 and the corrosion parameters estimated using the Tafel extrapolation of the cathodic branch are summarized in Table 2. In the case of pure magnesium, corrosion parameters could not be determined due to the nonlinearity of the cathodic branch. It can be seen from the polarization curves that after 1 h exposure that the presence of both zinc and gadolinium in alloys shifts the corrosion potentials to more noble values, however, zinc effect is more pronounced. Both elements are more like noble metals than magnesium [43] and their addition to Mg increased the nobility of the resulting alloys. There were significant differences between the polarization curves measured for freshly prepared samples and those measured after 24 h. Firstly, corrosion potential after 24 h immersion was higher for all studied alloys compared with the corrosion potential after 1 h immersion. Secondly, hydrogen evolution as cathodic reaction is increased according cathodic curves for all specimens immersed for 24 h compared with those immersed for 1 h. After 24 h immersion, the surface of all samples was covered by corrosion products and the differences in corrosion potentials were almost negligible. After 1 h exposure, the corrosion rates estimated from current density were very similar, however, after 24 h immersion the corrosion rates of alloys were increased in the order Mg–1Zn < Mg–1Zn–3Gd < Mg–3Zn < Mg–3Zn–3Gd. Although corrosion current density of pure magnesium could not be estimated from curved cathodic branch, polarization curve was characterized by the lowest values of belonging current densities compared with other studied alloys. Therefore, we assume that the corrosion rate of Mg after 24 h immersion should be the lowest compared to other studied alloys.

4 Discussion

4.1 Influence of Zn and Gd on alloy structure

It is shown in Fig. 1 that both Zn and Gd affect the structure of alloys. According to the phase diagram of binary Mg–Zn (Fig. 9) the maximum solid solubility for zinc in α-Mg is 6.2 wt% at eutectic temperature and this value is reduced to nearly 1.5 wt% at laboratory temperature. This means that after solidification process of

Fig. 6 Surfaces of the
investigated alloys after
immersion tests **a** Mg-1Zn,
**b** Mg–3Zn, **c** Mg–1Zn–3Gd,
d Mg–3Zn–3Gd, **e** Mg
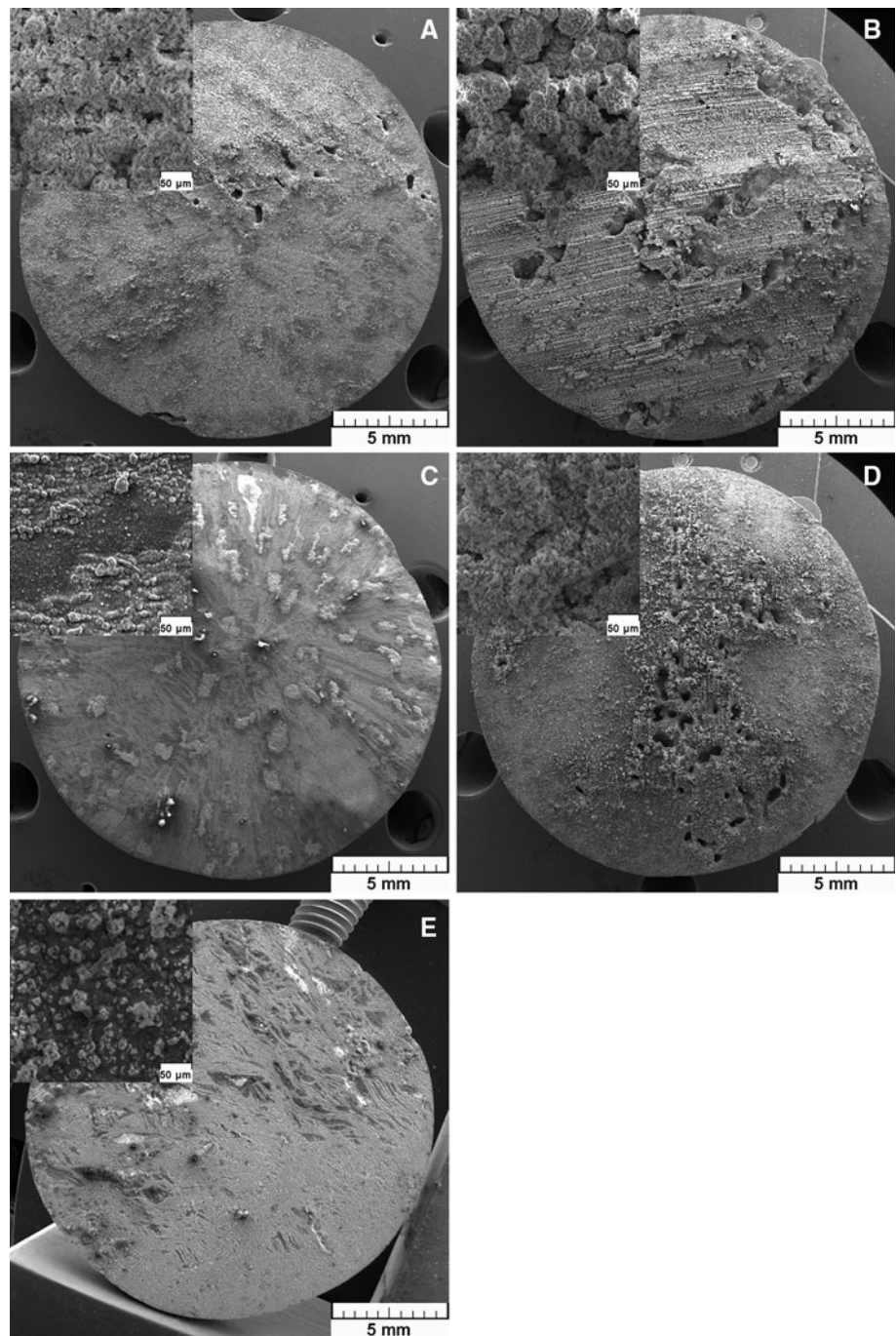
Mg–1Zn alloy only α-Mg should be presented in the structure. In our case non-equilibrium eutectic mixture of α-Mg and MgZn was formed during solidification process. Figure 1a, b show that the amount of MgZn eutectic phases in the structure of Mg–1Zn and Mg–3Zn binary alloys was increased with increasing Zn content. Moreover, the concentrations of Zn in the α-Mg solid solution at both dendrite cores and dendrite edges were increased for the alloys with higher quantities of zinc (Fig. 2).The concentration of zinc in α-Mg above maximum solubility limits especially

at the dendrite edges was caused by quite high cooling rate during casting. Similar results as in our study were reported in [21], where authors studied Mg–6Zn alloy in the cast state.

Based on the XRD and EDS analyses, only α-Mg and Mg$_5$Gd phases were observed in the Mg–1Zn–3Gd alloy. Compared with Mg–1Zn binary alloy, the concentration of Zn in the dendrites was slightly decreased. We consider two main reason: 1. Some amount of Zn is dissolved in the Mg$_5$Gd phase where it can act as a substitute for Mg atoms

Fig. 7 Surfaces of the investigated alloys after immersion tests and removal of the corrosion products by soaking in a solution of 200 g/l CrO_3, 10 g/l $AgNO_3$ and 20 g/l $Ba(NO_3)_2$ **a** Mg–1Zn, **b** Mg–3Zn, **c** Mg–1Zn–3Gd, **d** Mg–3Zn–3Gd, **e** Mg
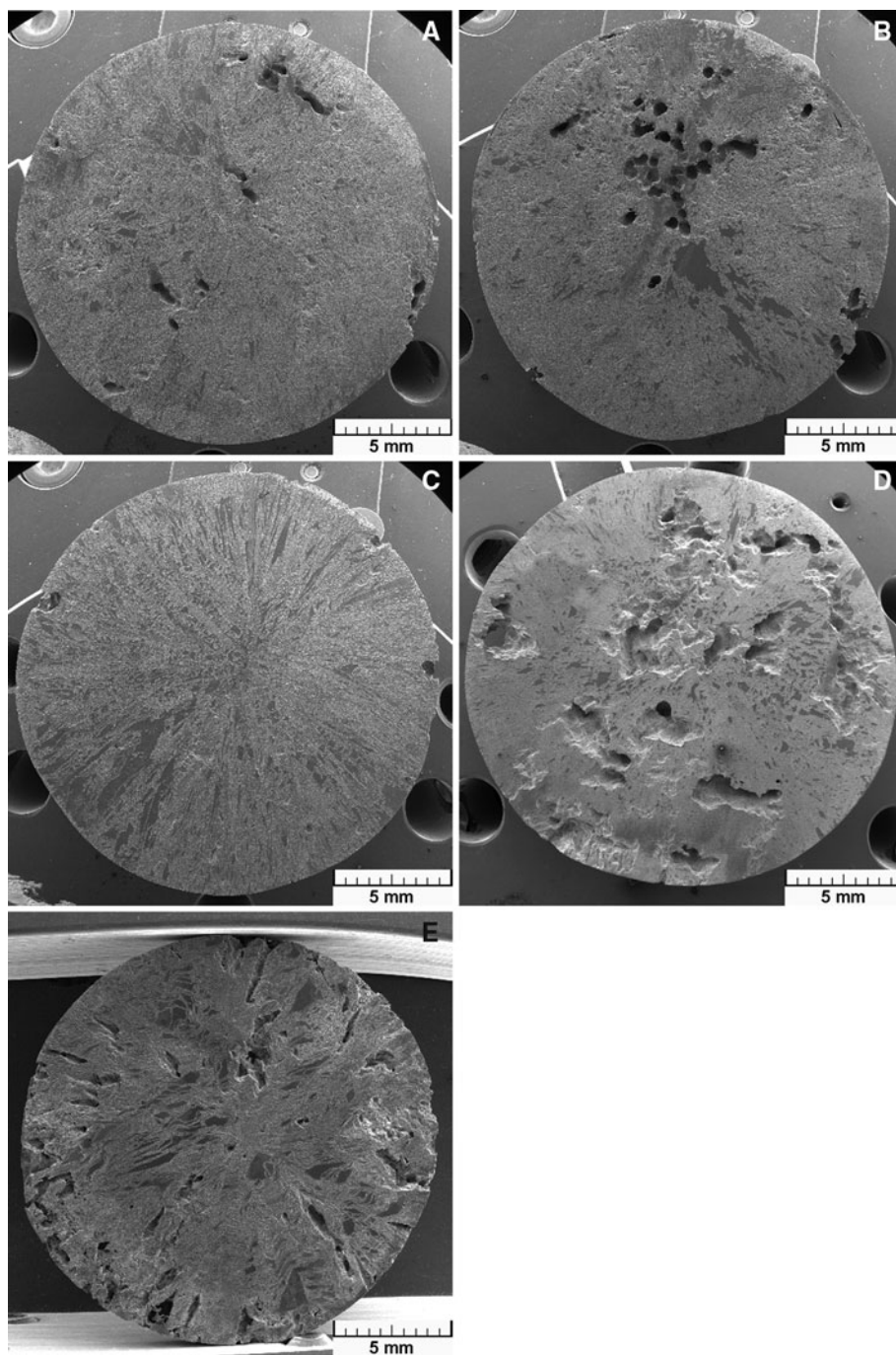
[44], 2. Total amount of Zn in Mg–1Zn–3Gd alloy is a bit lower compared to Mg–1Zn alloy. In [45], ternary magnesium alloy with 5 wt% of Gd and 1 wt% of Zn was studied. This alloy contained only Mg_5Gd phases and was characterized by obvious Zn segregation which are comparable data with our results. On the contrary, in [46] authors studied Mg-2.74Gd-1.06Zn (wt%) alloy in the state of rolled sheets and found both Mg_5Gd and $Mg_3Gd_2Zn_3$ phases. However, in this case presence of ternary phase can be connected with heat mechanical processing. We assume

that due to the close atomic ratio of Mg and Zn, majority of Zn is preferentially dissolved in α-Mg, and therefore, no ternary phases are formed.

Mg–3Zn–3Gd alloy contained the highest volume fraction of intermetallic phases that were identified as $Mg_3Gd_2Zn_3$ (W-phase) and Mg_5Gd. Qi et al. [44] thermodynamically modeled Mg–Zn–Gd system at 400 °C. According to their results, the composition of Mg–3Zn–3Gd alloy is in the two phase region containing α-Mg and W-phase. In their simulation for the non-equilibrium
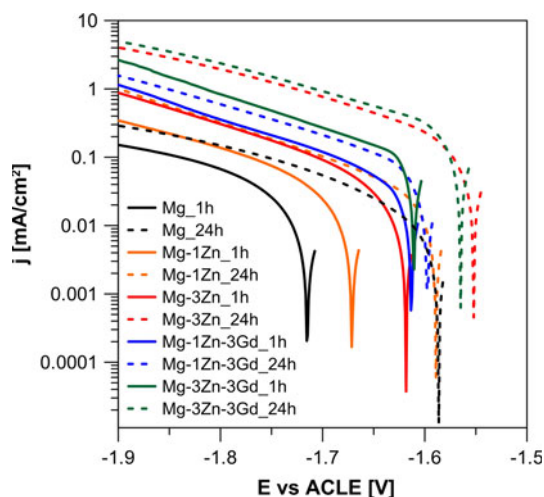
**Fig. 8** Potentiodynamic curves of pure Mg, Mg–3Zn and Mg–3Zn–3Gd alloys

solidification of Mg-5at.% Zn-0.5 at.% Gd they assume firstly the formation of α-Mg and W-phase and later, at lower temperatures, other phase transformations can take place. Therefore, it is possible that at higher cooling rates W-phase can be present in the structure as thermodynamically non-equilibrium phase. Although we are not sure that W-phase is equilibrium phase at our composition at laboratory temperatures, other studies confirmed its presence at structure [42, 45–49]. Yong et al. [48] tried to change the Zn/Gd (at.%) ratio in Mg–Zn–Gd system and studied the formation of intermetallic phases. They found that W-phase and an unidentified phase were in the cast state of alloys with Zn/Gd ratio (at.%) from 0.25–1. Although the composition of our Mg–3Zn–3Gd alloy corresponds to Zn/Gd (at.%) ratio of 2.63, the major identified phase was still $Mg_3Gd_2Zn_3$. However, the similar results were published in [46], where structure of ZG11 alloy with Zn/Gd (at.%)

Table 2 Corrosion parameters of the as-cast alloys determined from the potentiodynamic measurements

	1 h				24 h			
	E_{cor} [V]	β_C [V/dec]	j_0 [A/cm^2]	v_i [mm/y]	Ecor [V]	β_C [V/dec]	j_0 [A/cm^2]	v_i [mm/y]
Mg–1Zn	−1.67	0.201	4.31×10^{-5}	0.92	−1.59	0.202	2.88×10^{-5}	0.64
Mg–3Zn	−1.62	0.217	4.43×10^{-5}	0.93	−1.55	0.234	1.99×10^{-4}	4.11
Mg–1Zn–3Gd	−1.61	0.23	5.55×10^{-5}	1.22	−1.60	0.222	7.22×10^{-5}	1.45
Mg–3Zn–3Gd	−1.61	0.201	9.22×10^{-5}	1.86	−1.56	0.245	3.11×10^{-4}	4.86

E_{cor} corrosion potential, I_0 corrosion current density, β_C Tafel slope of cathodic branch, v_i corrosion rate estimated using Tafel extrapolation

Fig. 9 The Mg–Zn binary phase diagram [55]
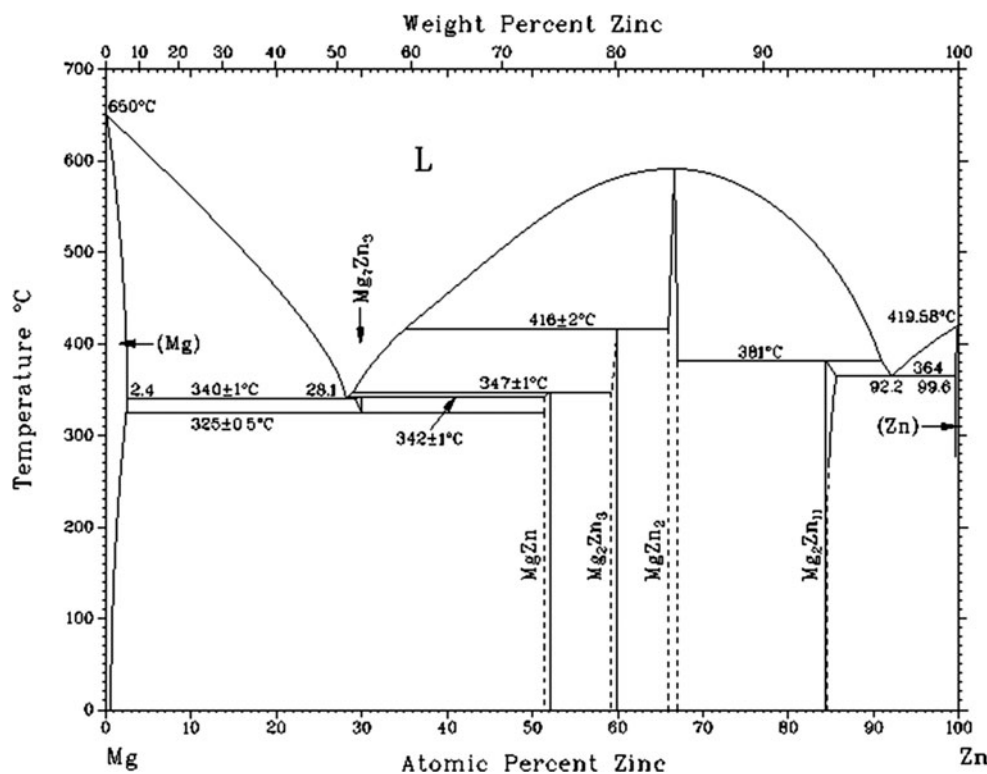
ratio 2.4 contained Mg₃Gd₂Zn₃ and α-Mg. Our results showed that the concentration of zinc in α-Mg was increased compared to Mg–1Zn–3Gd as a consequence of higher content of zinc in the Mg–3Zn–3Gd alloy. It is known that zinc has closer atomic radius to magnesium than gadolinium which allows easier formation of the solid solution of α-Mg [45]. For this reason gadolinium was preferentially concentrated in intermetallic phases and its concentration in solid solution was lower than in Mg–1Zn–3Gd alloy.

4.2 Influence of Zn and Gd on corrosion resistance

Figure 5 demonstrates that both Zn and Gd affect the corrosion resistance of Mg-based alloys. The addition of zinc improves the nobility of the magnesium alloys and shifts the corrosion potential to more positive values (Fig. 8). However, majority of Zn is concentrated in secondary phases that are formed in the structure. These phases act as cathodes and increase the corrosion rate because of the galvanic effect [50, 51]. If the Zn concentration is low (the Mg–1Zn alloy), the amount of MgZn intermetallics is low, which leads to a low corrosion rate of the alloy (Fig. 5) and only some observable local attacks are seen on the alloy surface (Fig. 6). An increase in the volume fraction of these secondary phases in the Mg–3Zn alloy has a detrimental effect on corrosion resistance because of an increase in the galvanic effect between the α-Mg matrix and MgZn phase (Fig. 1b). In the Mg–1Zn–3Gd alloy, the galvanic effect is weak. This is mainly for two reasons: (1) Mg–1Zn–3Gd alloy contained low volume fraction of the intermetallic phases (Fig. 1c). Moreover, these phases contained especially Gd which has a nobility closer to that of Mg compared to Zn [43]. (2) The Mg₅Gd phases are surrounded by a solid solution of α-Mg enriched by Zn and Gd, which decreases the difference in corrosion potentials at the interface of phases and the matrix. In contrast, the highest corrosion rate was measured for the Mg–3Zn–3Gd alloy. This alloy contained the highest amount of the ternary phase, creating a nearly continuous network along the dendrites (Fig. 1d). Because of high Zn and Gd concentrations in these phases, they act as cathodes and stimulate galvanic corrosion. In addition, the intermetallic phases are surrounded by a solid solution depleted of Zn and Gd (Fig. 2), which also contributes to the galvanic effect. Rare Earth elements are considered as suitable alloying elements for magnesium alloys because of its positive influence on corrosion resistance. It has been shown that their beneficial effect is especially connected with their presence in solid solution. On the contrary its presence in intermetallic phases may lead to the formation of galvanic cell. Concentration of Gd in Mg–1Zn–3Gd alloy in primary Mg is higher compared to Mg–3Zn–3Gd

alloy. This is probably next important fact, why the corrosion rate of Mg–Zn–3Gd is slower compared to Mg–3Zn–3Gd. After removing corrosion products surface condition of studied materials is in good relations to corrosion rates [Fig. 7] of studied alloys. It can be seen that the amount of pits or areas with signs of local corrosion increase for Mg–Zn and Mg–Zn–Gd alloys in order Mg–1Zn–3Gd, Mg–1Zn, Mg–3Zn, Mg–3Zn–3Gd. Although the surface layer on magnesium after immersion in physiological solution appears quite regularly, there are significant signs of localized corrosion that spread across the surface of the sample. Localized corrosion on pure magnesium has already been reported in literature [50].

The curves of the cathodic region represent the polarization behavior of non-corroded surface of the sample and the reaction of hydrogen evolution. Our measurements of polarization curves showed that there were significant differences for cathodic curves measured after 1 or 24 h immersion. As it has been reported in literature [52–54], at early exposure, the corrosion potential relates to the breakdown of the air formed film. Corrosion starts as localized corrosion and spread over the surface of the sample. During corrosion process the pH is increased especially at anodic sites that are preferentially dissolved. However, pH increase stimulate the formation of magnesium hydroxide, which can partially protect the area and, therefore, localized corrosion is partially suppressed. This is the reason, while the corroded surface of pure Mg is more or less covered by only shallow pits. In fact, this does not apply for other alloys because there is much more tendency for the initiation of micro galvanic corrosion. Although, during longer term immersion, resulting pits can be covered by corrosion products and can be observed only after pickling. After the steady state corrosion is achieved for all studied alloys, hydrogen evolution as cathodic process takes place on the corroded surface or corrosion products. According our results, hydrogen evolution from cathodic curves after 24 h immersion was obviously higher compared with 1 h immersion. This can be connected with two main facts. (1) Corrosion rate is increased after 24 h immersion. (2) The surface area is increased as a consequence of corrosion process. It is evident that corrosion rates estimated from the Tafel extrapolation of cathodic branches after one hour immersion are quite low and almost similar (Table 2). This suggests that after one hour immersion there is still the influence of air formed film for freshly prepared samples. After 24 h immersion, corrosion rates for Mg–3Zn and Mg–3Zn–3Gd were significantly increased, however, corrosion rate of Mg–1Zn–3Gd and Mg–1Zn remained almost the same. We assume that the initiation stage of the corrosion process in the case of Mg–3Zn and Mg–3Zn–3Gd is faster compared to other studied materials, which can be connected with the accelerating

effect of micro galvanic cell. There is not any exact relation among corrosion rates estimated using Tafel extrapolation and corrosion rates calculated from weight changes after 168 h immersion. However, both kind of results confirmed that Mg–1Zn and Mg–1Zn–3Gd alloys are more corrosion resistant materials due to the significantly lower corrosion rates compared to Mg–3Zn and Mg–3Zn–3Gd.

5 Conclusions

The following conclusions can be made from the presented study:

1. Zinc (1 and 3 wt.%) improves the corrosion resistance of as-cast Mg-based binary alloys.
2. Corrosion rate is influenced significantly by the amount of secondary phases that acts as cathodic sites and supports the galvanic effect among these phases and the magnesium matrix.
3. Addition of Gd to Mg–1Zn alloys decreases the corrosion rate to nearly 0.8 mm/y.
4. Addition of Gd to Mg–3Zn alloys has strong detrimental effects on corrosion resistance because of the galvanic effect that occurs between the continuous network of the ternary phase and the magnesium matrix.

References

1. Song G. Control of biodegradation of biocompatable magnesium alloys. Corros Sci. 2007;49(4):1696–701.
2. Seal CK, Vince K, Hodgson MA. Biodegradable surgical implants based on magnesium alloys – a review of current research. IOP Conference Ser Mater Sci Eng. 2009;4(1):012011.
3. Davis JR. Handbook of materials for medical devices. Materials Park: ASM International; 2003.
4. Wang X, Lu HM, Li XL, Li L, Zhenh YF. Effect of cooling rate and composition on microstructures and properties of Zn–Mg alloys. Trans Nonferr Met Soc China. 2007;17:S122–5.
5. Jürgen V. Magnesium: nutrition and metabolism. Mol Aspects Med. 2003;24(1–3):27–37.
6. Staiger MP, Pietak AM, Huadmai J, Dias G. Magnesium and its alloys as orthopedic biomaterials: a review. Biomaterials. 2006;27(9):1728–34.
7. Zeng R, Dietzel W, Witte F, et al. Progress and challenge for magnesium alloys as biomaterials, vol. 8. Weinheim: Wiley; 2008.
8. Witte F. The history of biodegradable magnesium implants: a review. Acta Biomater. 2010;6(5):1680–92.
9. Pereda MD, Alonso C, Burgos-Asperilla L, del Valle JA, Ruano OA, Perez P, et al. Corrosion inhibition of powder metallurgy Mg by fluoride treatments. Acta Biomater. 2010;6(5):1772–82.
10. Gray-Munro JE, Seguin C, Strong M. Influence of surface modification on the in vitro corrosion rate of magnesium alloy AZ31. J Biomed Mater Res A. 2009;91A(1):221–30.
11. Hiromoto S, Shishido T, Yamamoto A, Maruyama N, Somekawa H, Mukai T. Precipitation control of calcium phosphate on pure magnesium by anodization. Corros Sci. 2008; 50(10):2906–13.
12. Chun-Yan Z, Rong-Chang Z, Cheng-Long L, Jia-Cheng G. Comparison of calcium phosphate coatings on Mg–Al and Mg–Ca alloys and their corrosion behavior in Hank's solution. Surf Coat Technol. 2010;204(21–22):3636–40.
13. Erbel R, Di Mario C, Bartunek J, Bonnier J, de Bruyne B, Eberli FR, et al. Temporary scaffolding of coronary arteries with bio-absorbable magnesium stents: a prospective, non-randomised multicentre trial. Lancet. 2007;369(9576):1869–75.
14. Di Mario C, Griffiths HUW, Goktekin O, Peeters N, Verbist JAN, Bosiers M, et al. Drug-eluting bioabsorbable magnesium stent. J Interv Cardiol. 2004;17(6):391–5.
15. Peeters P, Bosiers M, Verbist J, Deloose K, Heublein B. Preliminary results after application of absorbable metal stents in patients with critical limb ischemia. J Endovasc Ther. 2005;12(1):1–5.
16. Chang J, Guo X, He S, Fu P, Peng L, Ding W. Investigation of the corrosion for Mg–xGd–3Y–0.4Zr (x = 6,8,10,12 wt%) alloys in a peak-aged condition. Corros Sci. 2008;50(1):166–77.
17. Rokhlin LL, Nikitina NI. Recovery after ageing of Mg–Y and Mg–Gd alloys. J Alloy Comp. 1998;279(2):166–70.
18. Hänzi AC, Gerber I, Schinhammer M, Löffler JF, Uggowitzer PJ. On the in vitro and in vivo degradation performance and biological response of new biodegradable Mg–Y–Zn alloys. Acta Biomater. 2010;6(5):1824–33.
19. Hort N, Huang Y, Fechner D, Stormer M, Blawert C, Witte F, et al. Magnesium alloys as implant materials-principles of property design for Mg–RE alloys. Acta Biomater. 2010;6(5):1714–25.
20. Xin Y, Hu T, Chu PK. In vitro studies of biomedical magnesium alloys in a simulated physiological environment: a review. Acta Biomater. 2011;7(4):1452–9.
21. Zhang S, Zhang X, Zhao C, Li J, Song Y, Xie C, et al. Research on an Mg–Zn alloy as a degradable biomaterial. Acta Biomater. 2010;6(2):626–40.
22. Witte F, Hort N, Vogt C, Cohen S, Kainer KU, Willumeit R, et al. Degradable biomaterials based on magnesium corrosion. Curr Opin Solid State Mater Sci. 2008;12(5–6):63–72.
23. http://ods.od.nih.gov/factsheets/Zinc-HealthProfessional/. Accessed 19 Dec 2012.
24. Li Z, Gu X, Lou S, Zheng Y. The development of binary Mg–Ca alloys for use as biodegradable materials within bone. Biomaterials. 2008;29(10):1329–44.
25. Zhang EL, Yang L, Xu JW, Chen HY. Microstructure, mechanical properties and bio-corrosion properties of Mg–Si(–Ca, Zn) alloy for biomedical application. Acta Biomater. 2010;6(5):1756–62.
26. Zhang E, Yang L. Microstructure, mechanical properties and bio-corrosion properties of Mg–Zn–Mn–Ca alloy for biomedical application. Mater Sci Eng A. 2008;497(1–2):111–8.
27. Gu XN, Zheng W, Cheng Y, Zheng YF. A study on alkaline heat treated Mg–Ca alloy for the control of the biocorrosion rate. Acta Biomater. 2009;5(7):2790–9.
28. Huan Z, Leeflang M, Zhou J, Fratila-Apachitei L, Duszczyk J. In vitro degradation behavior and cytocompatibility of Mg–Zn–Zr alloys. J Mater Sci Mater Med. 2010;21(9):2623–35.
29. Gu X, Zheng Y, Zhong S, Xi T, Wang J, Wang W. Corrosion of, and cellular responses to Mg–Zn–Ca bulk metallic glasses. Biomaterials. 2010;31(6):1093–103.
30. Zberg B, Uggowitzer PJ, Loffler JF. MgZnCa glasses without clinically observable hydrogen evolution for biodegradable implants. Nat Mater. 2009;8(11):887–91.
31. Zhang E, He W, Du H, Yang K. Microstructure, mechanical properties and corrosion properties of Mg–Zn–Y alloys with low Zn content. Mat Sci Eng A. 2008;488(1–2):102–11.

32. Nie JF, Gao X, Zhu SM. Enhanced age hardening response and creep resistance of Mg–Gd alloys containing Zn. Scripta Mater. 2005;53(9):1049–53.

33. Yuan G, Kato H, Amiya K, Inoue A. Excellent creep properties of Mg-Zn-Cu-Gd-based alloy strengthened by quasicrystals and Laves phases. J Mater Res. 2005;20(5):1278–86.

34. Liu Y, Yuan G, Ding W, Lu C. Deformation behavior of Mg–Zn–Gd-based alloys reinforced with quasicrystal and Laves phases at elevated temperatures. J Alloy Comp. 2007;427(1–2):160–5.

35. Massalski B, Okamoto H. Binary alloys phase diagrams. 2nd ed. Materials Park: ASM International; 1996.

36. Liu Y, Yuan GY, Lu C, Ding WJ. Progress in light metals, aerospace materials and superconductors. Mat Sci Forum. 2007;546–549:323–6.

37. Xu DK, Tang WN, Liu L, Xu YB, Han EH. Effect of Y concentration on the microstructure and mechanical properties of as-cast Mg–Zn–Y–Zr alloys. J Alloy Comp. 2007;432(1–2):129–34.

38. Liu K, Zhang J, Rokhlin LL, Elkin FM, Tang D, Meng J. Microstructures and mechanical properties of extruded Mg–8Gd–0.4Zr alloys containing Zn. Mater Sci Eng A. 2009;505(1–2):13–9.

39. Wu S, Gao JC, Qiao LY, Wang Y. Corrosion behavior of Mg and Mg–Zn alloys in simulated body fluid. Trans Nonferr Met Soc China. 2008;18(3):588–92.

40. Wu D, Chen RS, Han EH. Excellent room-temperature ductility and formability of rolled Mg–Gd–Zn alloy sheets. J Alloy Comp. 2011;509(6):2856–63.

41. Friedrich HE, Mordike BL. Magnesium technology. Berlin: Springer; 2006.

42. Yang J, Wang L, Wang L, Zhang H. Microstructures and mechanical properties of the Mg–4.5Zn–xGd (x = 0, 2, 3 and 5) alloys. J Alloy Comp. 2008;459(1-2):274–80.

43. Millazo G, Caroli S, Sharma VK. Tables of standart electrode potentials. Chichester: Wiley; 1978.

44. Qi HY, Huang GX, Bo H, Xu GL, Liu LB, Jin ZP. Experimental investigation and thermodynamic assessment of the Mg–Zn–Gd system focused on Mg-rich corner. J Mater Sci. 2011;47(3):1319–30.

45. Balasubramani N, Pillai UTS, Pai BC. Effect of Zn concentration on the microstructure and phase formation of Mg–5Gd alloy. J Alloy Comp. 2008;460(1–2):L6–10.

46. Chen R, Liang S, Wu D, Han E. Consideration of castability and formability for new magnesium alloys. Open J Met. 2012;2(1):8–17.

47. Liu Y, Yuan G, Lu C, Ding W. Stable icosahedral phase in Mg–Zn–Gd alloy. Scripta Mater. 2006;55(10):919–22.

48. Yong L, Guangyin Y, Song Z, Xinping Z, Chen L, Wenjiang D. Effects of Zn/Gd ratio and content of Zn, Gd on phase constitutions of Mg alloys. Mater Trans. 2008;49(5):941–4.

49. Li JH, Schumacher P. Solidification and age hardening behaviour of Mg–Zn–Gd Alloys. IOP Conf Ser Mater Sci Eng. 2012;27(1):012021.

50. Song Y, Han E-H, Shan D, Yim CD, You BS. The effect of Zn concentration on the corrosion behavior of Mg–xZn alloys. Corros Sci. 2012;65:322–30.

51. Song Y, Han E-H, Shan D, Yim CD, You BS. The role of second phases in the corrosion behavior of Mg–5Zn alloy. Corros Sci. 2012;60:238–45.

52. Shi Z, Liu M, Atrens A. Measurement of the corrosion rate of magnesium alloys using Tafel extrapolation. Corros Sci. 2010;52(2):579–88.

53. Atrens A, Liu M, Zainal Abidin NI. Corrosion mechanism applicable to biodegradable magnesium implants. Mater Sci Eng B. 2011;176(20):1609–36.

54. Zhao M-C, Schmutz P, Brunner S, Liu M, Song G-l, Atrens A. An exploratory study of the corrosion of Mg alloys during interrupted salt spray testing. Corros Sci. 2009;51(6):1277–92.

55. Gale WF, Totemeier TC. Smithells metals reference book. 8th ed. Amsterdam: Elsevier; 2004.